Journal of Biomolecular NMR, **11:** 135–152, 1998.
KLUWER/ESCOM

Differential isotope labeling strategy for determining the structure of myristoylated recoverin by NMR spectroscopy

Toshiyuki Tanaka[a], James B. Ames[b], Masatsune Kainosho[c], Lubert Stryer[b] & Mitsuhiko Ikura[a,d,*]

[a]*Center for Tsukuba Advanced Research Alliance and Institute of Applied Biochemistry, University of Tsukuba, Tsukuba 305, Japan;* [b] *Department of Neurobiology, Stanford University School of Medicine, Stanford, CA 94305, U.S.A.;* [c] *Department of Chemistry, Tokyo Metropolitan University, Hachiouji 192-03, Japan;* [d]*Division of Molecular and Structural Biology, Ontario Cancer Institute and Department of Medical Biophysics, University of Toronto, 610 University Avenue, Toronto, ON, Canada M5G 2M9*

Received 22 May 1997; Accepted 30 July 1997

Key words: calcium-myristoyl switch, multidimensional heteronuclear magnetic resonance, recoverin, solution structure

Abstract

The three-dimensional solution structure of recombinant bovine myristoylated recoverin in the Ca^{2+}-free state has been refined using an array of isotope-assisted multidimensional heteronuclear NMR techniques. In some experiments, the myristoyl group covalently attached to the protein N-terminus was labeled with ^{13}C and the protein was unlabeled or vice versa; in others, both were ^{13}C-labeled. This differential labeling strategy was essential for structural refinement and can be applied to other acylated proteins. Stereospecific assignments of 41 pairs of β-methylene protons and 48 methyl groups of valine and leucine were included in the structure refinement. The refined structure was constructed using a total of 3679 experimental NMR restraints, comprising 3242 approximate interproton distance restraints (including 153 between the myristoyl group and the polypeptide), 140 distance restraints for 70 backbone hydrogen bonds, and 297 torsion angle restraints. The atomic rms deviations about the averaged minimized coordinate positions for the secondary structure region of the N-terminal and C-terminal domains are 0.44 ± 0.07 and 0.55 ± 0.18 Å for backbone atoms, and 1.09 ± 0.07 and 1.10 ± 0.15 Å for all heavy atoms, respectively. The refined structure allows for a detailed analysis of the myristoyl binding pocket. The myristoyl group is in a slightly bent conformation: the average distance between C1 and C14 atoms of the myristoyl group is 14.6 Å. Hydrophobic residues Leu^{28}, Trp^{31}, and Tyr^{32} form a cluster that interacts with the front end of the myristoyl group (C1–C8), whereas residues Phe^{49}, Phe^{56}, Tyr^{86}, Val^{87}, and Leu^{90} interact with the tail end (C9–C14). The relatively deep hydrophobic pocket that binds the myristoyl group (C14:0) could also accommodate other naturally occurring acyl groups such as C12:0, C14:1, and C14:2 chains.

Introduction

Recoverin, a 23 kDa retinal protein, serves as a calcium sensor in vision. It belongs to the EF-hand superfamily represented by calmodulin and troponin C and contains four EF-hand motifs. Only two of the EF-hands have the ability to bind Ca^{2+} ions (Flaherty et al., 1993; Ames et al., 1995a). The Ca^{2+}-bound form of recoverin prolongs the visual photoresponse (Gray-Keller et al., 1993), most likely by blocking phosphorylation of photoexcited rhodopsin (Kawamura et al., 1993). Recent studies have shown that Ca^{2+}-bound recoverin binds to and inhibits rhodopsin kinase and that recoverin is critical for Ca^{2+}-sensitive activity of the kinase (Chen et al., 1995; Klenchin et al., 1995).

* To whom correspondence should be addressed.

Abbreviations: CT, constant time; *E. coli*, *Escherichia coli*; NMT, *N*-myristoyl-CoA transferase; PFG, pulse field gradient; rms, root mean square.

Retinal recoverin contains a covalently attached myristoyl or related acyl group at its N-terminus (Dizhoor et al., 1992). Ca^{2+} binding to myristoylated, not unmyristoylated, recombinant recoverin induces the translocation of the protein from cytosol to membranes (Zozulya and Stryer, 1992; Dizhoor et al., 1993), suggesting that the myristoyl group is crucial for membrane targeting and that recoverin possesses a Ca^{2+}-myristoyl switch. Indeed, recent NMR studies have demonstrated that the binding of calcium to recoverin induces extrusion of the myristoyl group into the solvent (Ames et al., 1995b; Hughes et al., 1995), making the myristoyl group available to insert into lipid bilayers or bind to target proteins.

Several homologues of recoverin have been discovered recently that most likely possess a Ca^{2+}-myristoyl switch. The closest relatives of recoverin are S-modulin (Kawamura, 1993) in frog rods and visinin (Yamagata et al., 1990) in chicken cones which are 83% and 59% identical to recoverin. Many homologues such as hippocalcin (Kobayashi et al., 1992), several neurocalcins (Terasawa et al., 1992), NVPs (neural visinin-like proteins) (Kuno et al., 1992), and frequenin (Pongs et al., 1993) are expressed in the central nervous system and are about 50% identical in sequence to recoverin. The exact function of the homologues is not known, although they most likely regulate the deactivation of seven helix receptors. All homologues possess a myristoylation consensus sequence (GXXXSX) at their N-termini (Towler et al., 1988), and several are found to be acylated (Yamagata et al., 1990; Kuno et al., 1992; Terasawa et al., 1992; Kobayashi et al., 1993). Hippocalcin and neurocalcin have been shown to exhibit the Ca^{2+}-dependent membrane binding (Kobayashi et al., 1993; Ladant, 1995). The Ca^{2+}-myristoyl switch may be a common signature of all homologues.

The X-ray crystal structure of unmyristoylated recombinant recoverin has been solved at 1.9 Å resolution (Flaherty et al., 1993). Four EF-hand motifs are arranged in a compact array that contrasts with the dumbbell shape of calmodulin and troponin C. The four EF-hands are grouped into two domains: the N-terminal domain contains EF-1 and EF-2, and the C-terminal domain contains EF-3 and EF-4. The linker between the two domains is U-shaped rather than α-helical. Ca^{2+} is bound to EF-3 and Sm^{3+} (used as an isomorphous heavy atom for phasing) is bound to EF-2. The other two EF-hands do not bind Ca^{2+}. EF-1 contains a cysteine and proline in the binding loop that prevents the binding of Ca^{2+}. EF-4 is disabled by a salt bridge between Lys^{161} and Glu^{171}. Furthermore, these two EF-hands lack two essential acidic residues in EF-hand consensus sequence, which is crucial for Ca^{2+} coordination.

The crystal structure of unmyristoylated recoverin does not address the structural role of the myristoyl group and therefore raises the following questions: Does the myristoyl group stabilize any structure at the N-terminus and does it induce overall conformational changes to the protein? Also, what is the location of the myristoyl group? The myristoylated protein has thus far eluded crystallization. Consequently, we have turned to NMR spectroscopy to solve the structure of myristoylated recoverin, the physiologically relevant species. An efficient expression system of myristoylated recoverin developed by Zozulya and Stryer (1992) allows ^{13}C and ^{15}N labeling not only to the polypeptide but also to the myristoyl group, which is requisite for multidimensional NMR. We have previously reported the backbone ^{1}H, ^{15}N, and ^{13}C resonance assignments of recoverin and the elucidation of its secondary structure (Ames et al., 1994), and also the determination of a medium-resolution tertiary structure based on 2710 interatomic distance constraints (Tanaka et al., 1995). Here, we present a higher resolution tertiary structure of recoverin obtained from further analysis of NOEs and stereospecific assignments of β-methylenes, which resulted in 3242 interatomic distance constraints. A differential isotope labeling strategy to study lipidated proteins will be described.

Materials and methods

Sample preparation

Uniformly (>95%) ^{15}N- or $^{15}N/^{13}C$-labeled bovine recombinant recoverin with a non-labeled myristoyl group covalently attached to its N-terminus (Figure 1a) was prepared as described previously (Ames et al., 1994) except that myristic acid was added to the medium 1 h before the induction of NMT to give a final concentration of 5 mg l^{-1}. $^{13}C_{14}$-myristic acid (Isotec, Miamisburg, OH) was used instead for preparing uniformly ^{15}N- or ^{13}C-labeled protein with a ^{13}C-labeled myristoyl group (Figures 1b and c).

Stereospecifically ^{13}C-labeled leucine or valine was used to prepare the protein sample for the stereospecific assignments of methyls of leucine or valine. An *E. coli* strain DH5a containing plasmids pTREC2 and pBB131 was grown on the minimal

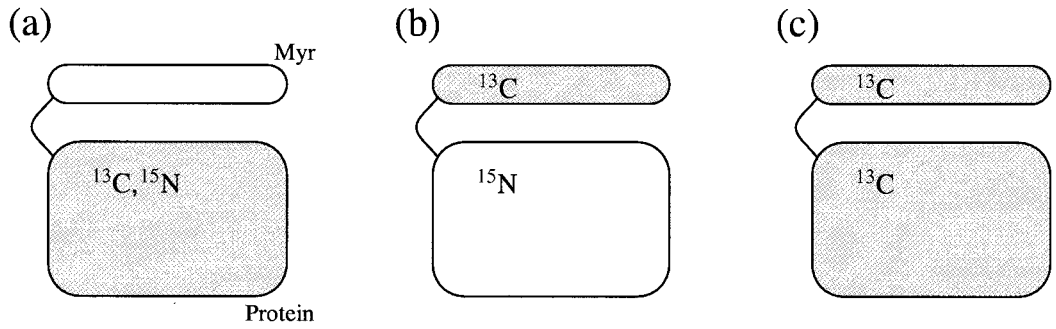

Figure 1. Schematic representation of the three different types of a myristoylated protein labeled with ^{13}C and/or ^{15}N. The uniformly ^{13}C-labeled part is shaded.

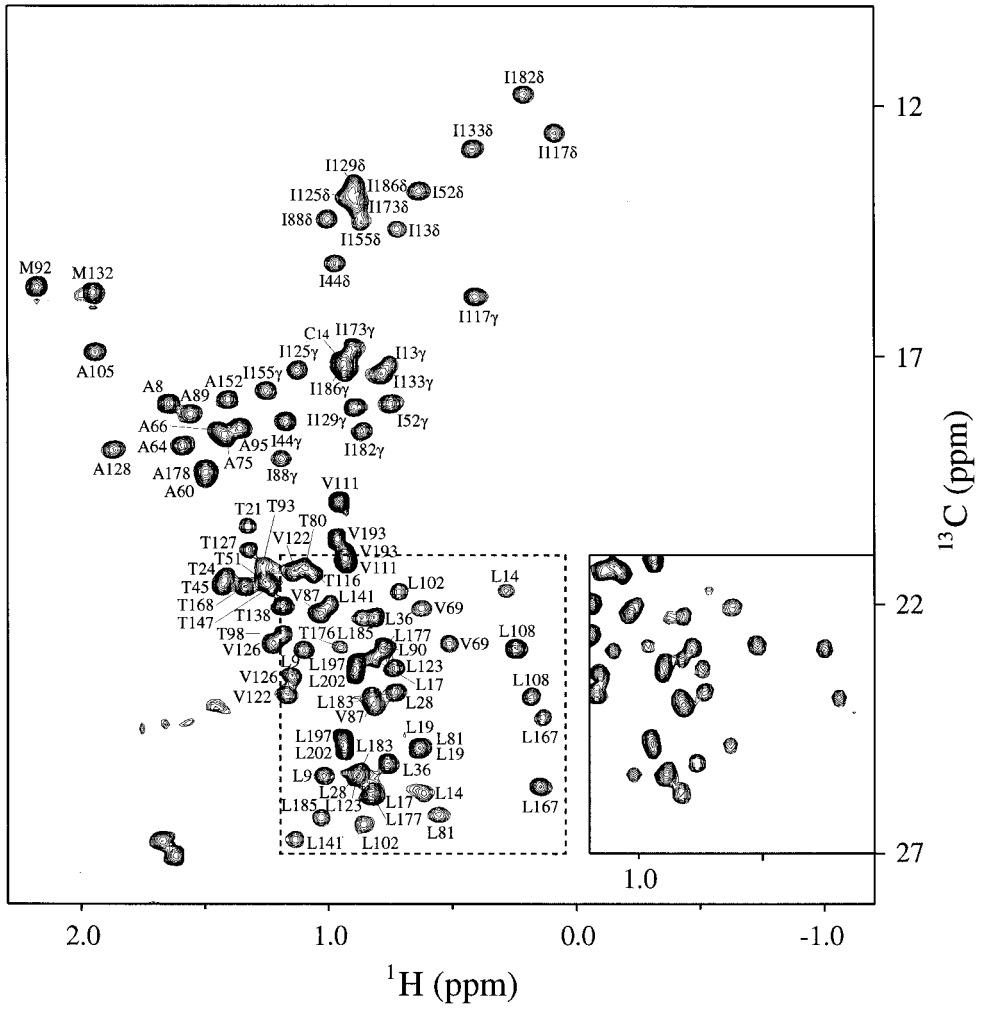

Figure 2. The methyl region of the 2D ^1H-^{13}C CT-HSQC spectrum of uniformly ^{13}C-labeled Ca^{2+}-free, myristoylated recoverin with the ^{13}C-labeled myristoyl group. The peaks are labeled with a sequence-specific assignment. Methionine methyls are shown in the same sign with other methyl signals. The inset shows the leucine and valine methyl region of the uniformly ^{13}C-labeled protein with the non-labeled myristoyl group.

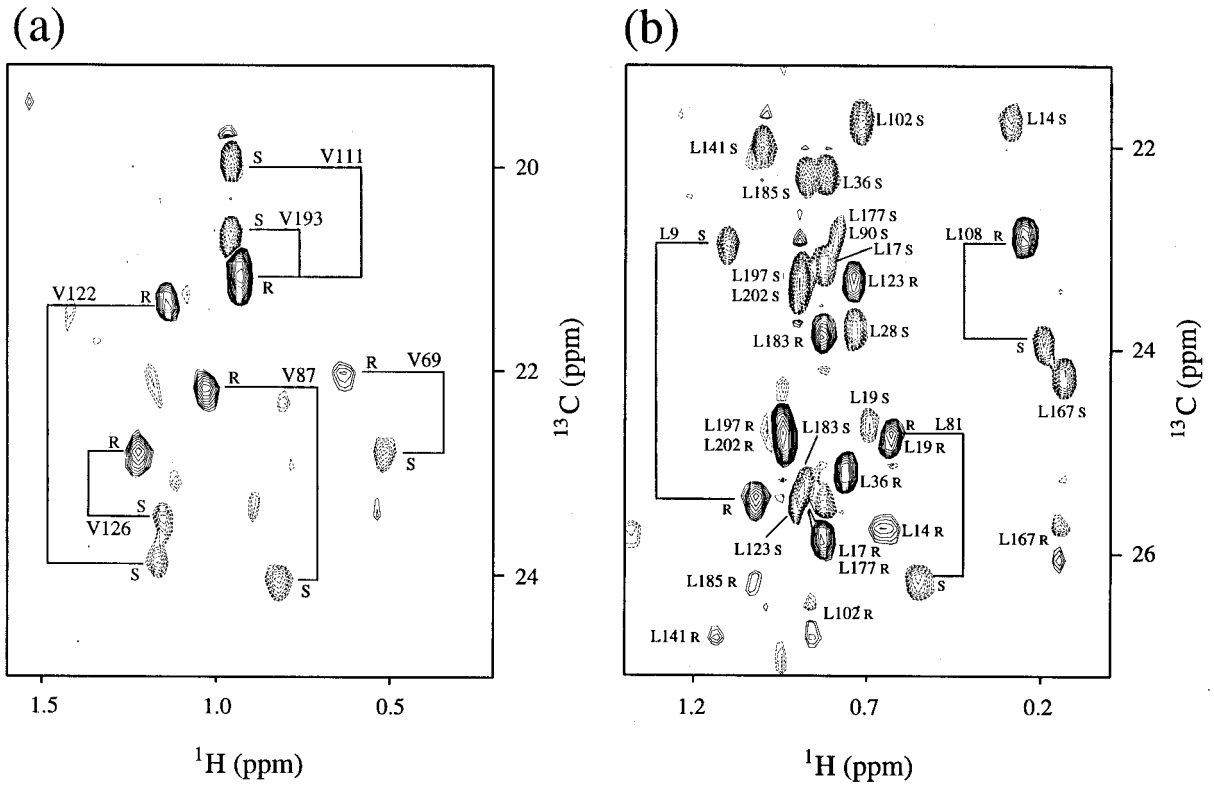

Figure 3. The methyl region of the 2D ^{1}H-^{13}C CT-HSQC spectrum of Ca^{2+}-free, myristoylated recoverin labeled with stereospecifically ^{13}C-labeled valine (a) or leucine (b). The peaks are labeled with both sequence-specific and stereospecific assignment. Positive contour levels (pro-R) are shown as solid lines and negative levels (pro-S) as dashed contours.

medium enriched with amino acids except for valine or leucine. ^{13}C-labeled leucine or valine was added 15 min before the induction of NMT by isopropyl β-D-thiogalactoside. After 1 h induction of NMT, recoverin expression was induced by raising the temperature to 42 °C and cells were grown at 42 °C for 2 h. Cells were then spun down, harvested, and stored at –70 °C.

The protein was purified as described previously (Zozulya and Stryer, 1992). Samples for NMR experiments were prepared by dissolving lyophilized protein in 0.5 ml of a 95% H_2O/5% D_2O (v/v) or 99.996% D_2O solution containing 100 mM KCl, 10 mM [D_{10}]-dithiothreitol, and 1 mM [D_{12}]-EDTA. Sample pH was adjusted to 6.8–7.0 with dilute NaOD. Protein concentrations were in the range 1.0–1.5 mM.

NMR measurements

All NMR spectra were recorded at 30 °C, unless otherwise noted, on a four-channel UNITY-plus 500 spectrometer equipped with an actively z gradient shielded triple-resonance probe and a PFG driver. PFG was employed to suppress spectral artifacts and minimize the intense water signal (Bax and Pochapsky, 1992). In all amide proton detected experiments, PFG was also used to select the coherence transfer pathways for sensitivity enhancement (Kay et al., 1992). All data were processed using the software NMRPipe and NMRDraw (Delaglio, 1993), and the data analysis was assisted by the software Capp and Pipp (Garrett et al., 1991). NMR assignments have been deposited with the BioMagResBank under accession number 4030.

Two-dimensional (2D) ^{1}H-^{13}C HMQC (Bendall et al., 1983) and ^{1}H-^{13}C CT-HSQC (Vuister and Bax, 1992) spectra were recorded with the following numbers of complex points and acquisition times: ^{13}C (F_1) 512, 51 ms, ^{1}H (F_2) 416, 52 ms with 32 transients for HMQC and ^{13}C (F_1) 128, 26 ms, ^{1}H (F_2) 416, 52 ms with 32 transients for CT-HSQC. Two-dimensional (Hβ)Cβ(CγCδ)Hδ and (Hβ)Cβ(CγCδCϵ)Hϵ experiments (Yamazaki et al., 1993) were recorded. The following numbers of complex points and acquisition times were used for both experiments: ^{13}C (F_1) 64, 8 ms, ^{1}H (F_2) 512, 64 ms (512 transients). A 2D

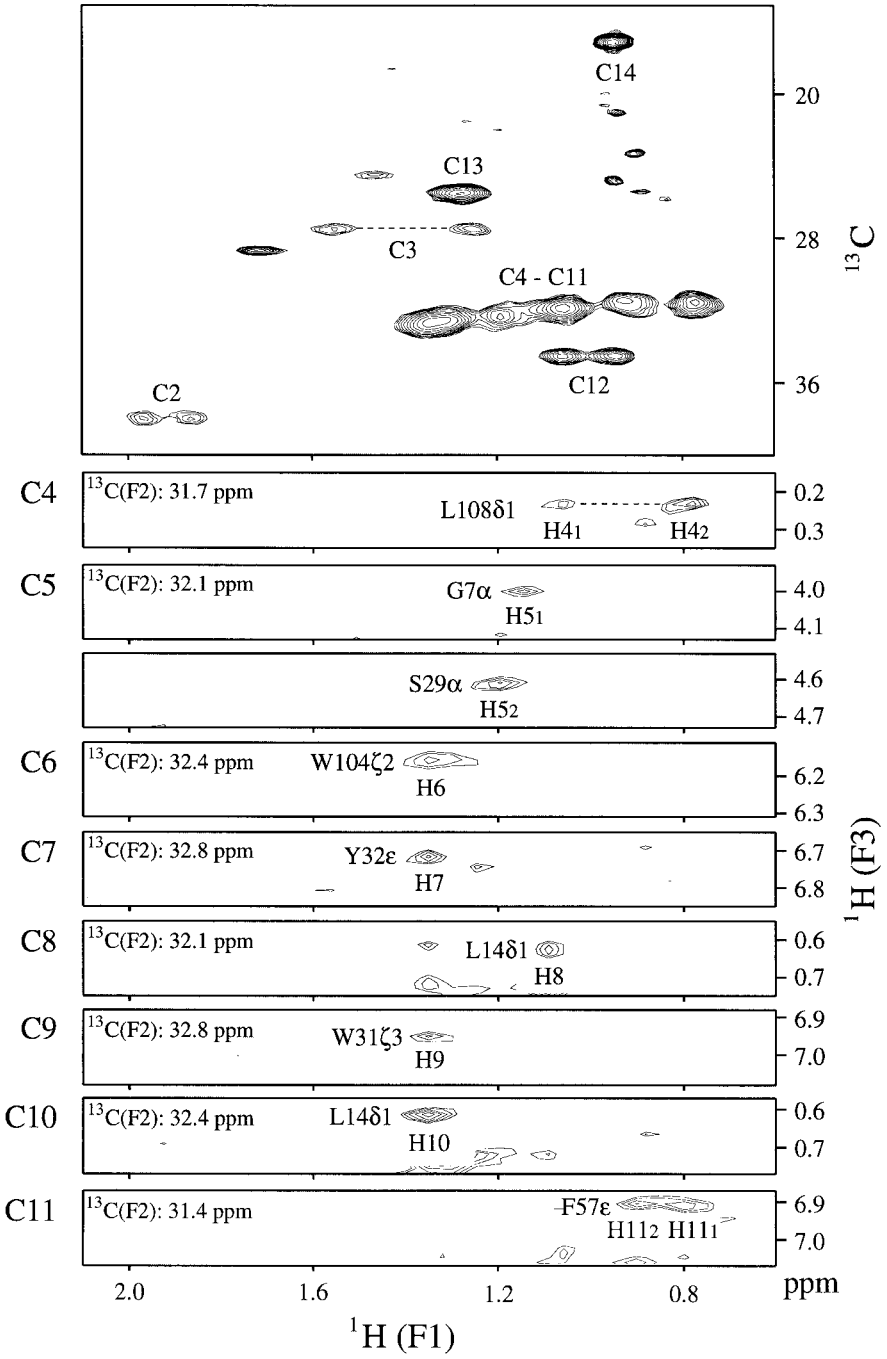

Figure 4. Two-dimensional ^{1}H-^{13}C HMQC spectrum of Ca^{2+}-free, myristoylated recoverin with the ^{13}C-labeled myristoyl group showing the near degeneracy of C4–C11 carbon and proton chemical shifts (top), and the slices of the 3D [^{13}C/F$_1$]-edited [^{13}C/F$_3$]-filtered HMQC-NOESY spectrum of the same sample, with whose help the assignment of C4–C11 was accomplished.

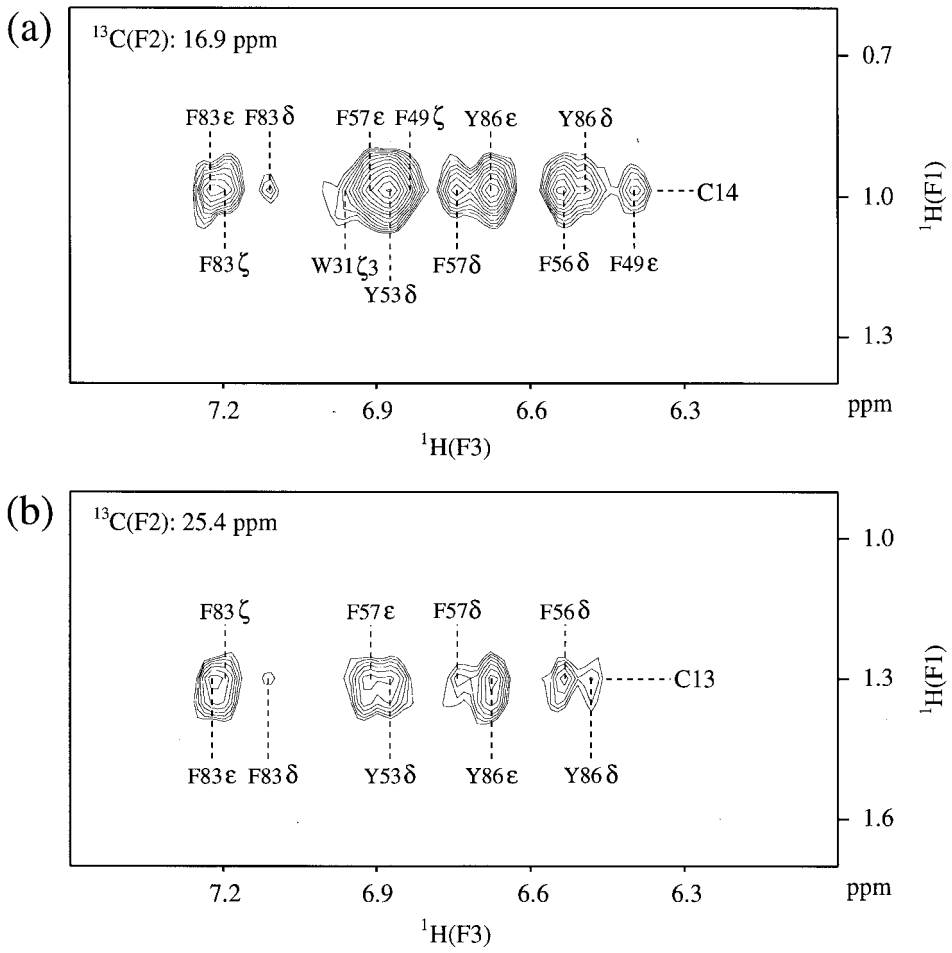

Figure 5. Slices of the 3D [^{13}C/F_1]-edited [^{13}C/F_3]-filtered HMQC-NOESY spectrum of Ca^{2+}-free, myristoylated recoverin labeled with the ^{13}C-labeled myristoyl group. NOE cross peaks between the aromatic protons of protein and the C14 methyl (a) or C13 methylene (b) protons of the myristoyl group are shown.

^{1}H/^{15}N HMQC-J (Kay and Bax, 1990) spectrum was recorded as described previously (Ames et al., 1994).

Homonuclear 2D NOESY (Jeener et al., 1979) and TOCSY (Braunschweiler and Ernst, 1983) spectra were recorded on a UNITY-600 spectrometer. The following numbers of complex points and acquisition times were used for both experiments: ^{1}H (F_1) 512, 64 ms, ^{1}H (F_2) 512, 64 ms (128 transients). For the NOESY experiments, mixing times of 50 and 100 ms were used. A WALTZ16 (Shaka et al., 1983) sequence was used in the TOCSY experiment with a mixing time of 41 ms.

A three-dimensional (3D) HCCH-COSY (Ikura et al., 1991) spectrum on the sample whose protein part is labeled with ^{15}N and the myristoyl group with ^{13}C (Figure 1b) was recorded with the following numbers of complex points and acquisition times: ^{1}H (F_1) 96, 27 ms, ^{13}C (F_2) 22, 7 ms, ^{1}H (F_3) 416, 52 ms (16 transients). A 3D HCCH-TOCSY (Bax et al., 1990; Kay et al., 1993) spectrum with a mixing time of 7 or 14 ms was recorded as described previously (Ames et al., 1994). An additional HCCH-TOCSY spectrum, whose ^{13}C carrier frequency was placed at the center of aromatic ring proton resonances (125 ppm), was recorded on a UNITY-600 spectrometer. The following numbers of complex points and acquisition times were used: ^{1}H (F_1) 64, 16 ms, ^{13}C (F_2) 32, 9 ms, ^{1}H (F_3) 416, 52 ms (16 transients).

A 3D simultaneous ^{15}N/^{13}C-edited NOESY-HSQC (Pascal et al., 1994) spectrum was recorded as described previously (Ames et al., 1994). Three-dimensional ^{15}N-edited NOESY-HSQC (Zhang et al.,

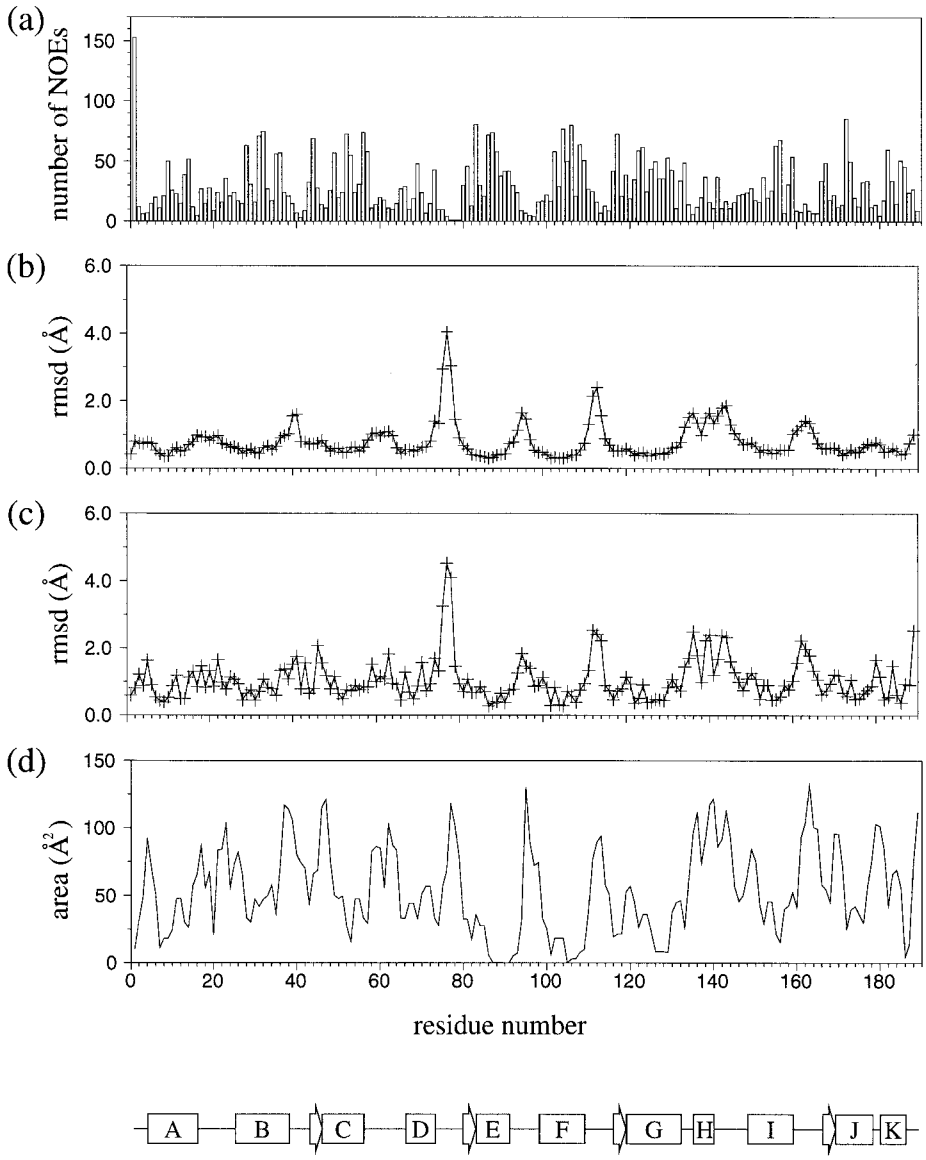

Figure 6. Structural data for the 30 NMR-derived Ca^{2+}-free, myristoylated recoverin structures plotted as a function of sequence. (a) NOE distribution, in which each interresidue NOE appears twice, once for each of the two interacting residues. (b, c) Average rms deviations from the average structure for backbone heavy atoms (N, C^{α}, C′ and O) and all heavy atoms, respectively, when atoms in regular secondary structure elements are fitted. (d) Solvent-accessible surface area smoothed over three residues (running average) calculated with X-PLOR (Brünger, 1992). At the bottom, cartoon representation of the secondary structure of Ca^{2+}-free, myristoylated recoverin is shown: α-helices are represented by boxes with labeling, and β-strands by open arrows.

1994) and ^{13}C-edited NOESY-HMQC (Muhandiram et al., 1993) spectra were recorded on a UNITY-600 spectrometer with the following numbers of complex points and acquisition times: ^{1}H (F_1) 128, 18 ms, ^{15}N (F_2) 32, 16 ms, ^{1}H (F_3) 512, 64 ms with 16 transients for ^{15}N-edited NOESY-HSQC and ^{1}H (F_1) 96, 23 ms, ^{13}C (F_2) 32, 11 ms, ^{1}H (F_3) 416, 52 ms with 16 transients for ^{13}C-edited NOESY-HMQC. A 3D [$^{13}C/F_1$]-edited [$^{13}C/F_3$]-filtered HMQC-NOESY (Lee et al., 1994) spectrum was recorded on a UNITY-600 spectrometer with the following number of complex points and acquisition times: ^{1}H (F_1) 64, 16 ms, ^{13}C (F_2) 30, 9 ms, ^{1}H (F_3) 416, 52 ms (64 transients). The mixing times were 100 ms for all 3D NOESY spectra, and

50 ms in addition for ^{15}N-edited NOESY-HSQC and ^{13}C-edited NOESY-HMQC spectra.

Three-dimensional HNHB (Archer et al., 1991) and ^{15}N-edited TOCSY-HMQC (Clore et al., 1991) spectra were recorded on a UNITY-600 spectrometer with the following numbers of complex points and acquisition times: ^{1}H (F_1) 64, 11 ms, ^{15}N (F_2) 32, 16 ms, ^{1}H (F_3) 512, 64 ms with 24 transients for HNHB and ^{1}H (F_1) 128, 18 ms, ^{15}N (F_2) 32, 16 ms, ^{1}H (F_3) 512, 64 ms with 16 transients for ^{15}N-edited TOCSY-HMQC. Heteronuclear $^{3}J_{NH\beta}$ coupling constants were estimated from a 3D HNHB spectrum and $^{3}J_{H\alpha H\beta}$ from a ^{15}N-edited TOCSY-HSQC spectrum with a mixing time of 49 ms. All coupling constants were estimated as small or large, corresponding with a *gauche* or *trans* orientation of the two nuclei.

Structural constraints

NOEs were assigned from 2D homonuclear and 3D heteronuclear NOESY spectra. Distance restraints between the myristoyl group and the protein were mainly obtained by ^{13}C-edited NOE spectra recorded on the sample whose N-terminal myristoyl group and protein are uniformly labeled with ^{13}C, and by a [^{13}C/F_1]-edited [^{13}C/F_3]-filtered HMQC-NOESY experiment on the sample whose protein portion is labeled with ^{15}N and the myristoyl group with ^{13}C. The upper distance bounds obtained from the NOESY spectra were grouped into four classes: 2.7, 3.3, 5.0, and 6.0 Å, respectively (2.9, 3.5, 5.0, and 6.0 Å for NOEs involving the backbone amide protons), corresponding to strong, medium, weak, and very weak NOEs. The lower bounds for the interproton distance restraints were set to the sum of the van der Waals radii of two protons. Upper distance limits for distances involving methyl protons and non-stereospecifically assigned methylene and aromatic protons were corrected for center averaging according to the method of Wüthrich et al. (1983), and an additional 0.5 Å was added to the upper distance limits for NOEs involving methyl protons (Clore et al., 1987; Wagner et al., 1987). Phi and psi dihedral angle restraints were derived from $^{3}J_{NH\alpha}$ coupling constants measured from the ^{1}H/^{15}N HMQC-J spectrum and chemical shift indices (Wishart and Sykes, 1994). Values of $-60 \pm 30°$ and $-40 \pm 30°$ were used for phi and psi dihedral angles, respectively, in α-helical regions, and $-120 \pm 30°$ and $120 \pm 60°$ in β-strands. The allowed range for χ_1 restraints was $\pm 35°$, which were derived from the conformational analysis based on stereospecific assignments of β-methylenes. Hydrogen bond restraints were obtained by analyzing the ^{1}H/^{2}H exchange rates and the NOE patterns characteristic of α-helices or β-strands. Two distance restraints, r_{NH-O} (1.8–2.3 Å) and r_{N-O} (2.3–3.3 Å), were used for each hydrogen bond.

Structure calculation

Structure calculations from residues 1 to 189 were performed using the YASAP protocol (Nilges et al., 1988) within X-PLOR (Brünger, 1992) as previously described (Bagby et al., 1994). The C-terminal 13 residues (190–202) were omitted from the calculation because of the lack of NOE observed. Calculations employed 3242 interproton distance restraints (comprising 995 intraresidue, 705 sequential, 568 short-range, 821 long-range, and 153 protein–myristate). These data were supplemented by 140 distance restraints for 70 hydrogen bonds identified on the basis of amide exchange and NOE data, and 297 dihedral angle restraints (127 ϕ, 109 ψ, and 61 χ_1). Fifty independent structures were calculated, and 30 structures with lowest total energy were selected.

The coordinates for the final structures will be deposited with the Protein Databank, Chemistry Department, Brookhaven National Laboratory, Upton, NY 11973, U.S.A.

Results

Resonance assignments

Recoverin is a relatively large protein for NMR analysis, consisting of 201 amino acids (plus the N-terminal myristoyl group) with 25 glutamic acids and 25 lysines. The backbone assignments were reported previously (Ames et al., 1994). The nearly complete assignments of side-chain signals except for those of leucines and aromatic residues have been made previously using the 3D HCCH-TOCSY with mixing times of 7 and 14 ms and ^{13}C-edited NOESY-HMQC spectra recorded on uniformly ^{13}C- and ^{15}N-labeled proteins with a non-labeled myristoyl group. Unexpectedly, almost no connectivities were observed for leucines except for Leu^{197} and Leu^{202} which are found in a flexible C-terminal region. The loss of connectivities for leucines was also seen in other ^{13}C-edited 3D spectra such as HNCACB and simultaneous ^{15}N/^{13}C-edited NOESY-HSQC. This resulted in incomplete assignments for leucine carbonyl, Cα, and Cβ atoms (less than 60%) in the previous study (Ames et al., 1994). This problem was overcome by using the ^{13}C-edited spectra of the sample whose protein and

myristoyl group are both uniformly labeled with ^{13}C. Two-dimensional ^{1}H-^{13}C CT-HSQC spectra of these two samples are shown in Figure 2. Many cross peaks assigned to leucine methyl groups (Leu^{14}, Leu^{81}, Leu^{167}, etc.) are clearly observed in the spectrum of the fully ^{13}C-labeled sample, whereas they are missing in the spectrum of the sample containing the non-labeled myristoyl group. The leucine side chains are most likely labeled with ^{13}C at a very low level in the sample containing the non-labeled myristoyl group.

The assignment of aromatic side chains is important for high-resolution NMR structure determination. Recoverin contains three histidines, 14 phenylalanines, three tryptophans, and five tyrosines. First, we performed 2D (Hβ)Cβ(CγCδ)Hδ and (Hβ)Cβ(CγCδCϵ)Hϵ experiments, which give the correlations from Cβ to Hδ and Hϵ, respectively. However, because of a severe overlap of Cβ chemical shifts and low sensitivity of these experiments, only one Hδ2 of histidines and three Hδ1 of tryptophans were assigned in this manner. The conventional method using the 2D TOCSY and NOESY experiments (Wüthrich, 1986) was more useful in assigning the rest of the aromatic proton resonances (only three aromatic protons were left unassigned). The carbon chemical shifts were obtained by the 2D ^{1}H-^{13}C CT-HSQC and HCCH-TOCSY spectra recorded with uniformly ^{13}C-labeled protein. Finally, most of the NMR observable ^{1}H (93%), ^{13}C (82%), and ^{15}N (97%) atoms of the protein were assigned.

Stereospecific assignment

Stereospecific NMR assignments improve the resolution of solution structure (Driscoll et al., 1989). In this study, we have attempted to stereospecifically assign β-methylenes of asparagine, aspartic acid, glutamic acid, leucine, lysine, phenylalanine, serine, tryptophan and tyrosine and methyl groups of leucine and valine. Out of 148 β-methylenes, 101 have distinct and well-resolved pairs of protons. A combination of two spin-spin coupling constants and two different NOE intensities was used to obtain the stereospecific assignments of β-methylenes: $^{3}J_{H\alpha H\beta}$ and $^{3}J_{NH\beta}$ coupling constants were estimated by qualitative analysis of H^{α}-H^{β} cross-peak intensities in a 3D ^{15}N-edited TOCSY-HMQC and HN-H^{β} cross-peak intensities in a 3D HNHB spectrum, respectively, and relative intensities of $d_{\beta N}$ and $d_{\alpha\beta}$ were obtained by examining 3D ^{15}N- and ^{13}C-edited NOESY-HMQC spectra with 50 ms mixing time, respectively. A homonuclear 2D NOESY spectrum with 50 ms mixing time was also used to obtain the information about $d_{\alpha\beta}$. Because of an ambiguity derived from spectral overlap, β-methylene protons were stereospecifically assigned only when three out of four NMR informations matched to one of the three χ_1 rotamers (+60°, +180°, and −60°). In this manner, 41 pairs of H^{β} protons were stereospecifically assigned. The χ_1 rotamers of valines, isoleucines, and threonines were also determined for 19 out of 31 residues using the torsion angle information.

Stereospecific assignments of leucine and valine methyl groups in recoverin were accomplished using the samples whose leucine or valine methyl groups were stereospecifically labeled with ^{13}C (Tate et al., 1995). In the case of valine, Cβ (Cγ for leucine) and CγR (CδR for leucine) are simultaneously enriched with ^{13}C at 85%, whereas CγS (CδS for leucine) is labeled at a much lower level (33%) (M. Kainosho, unpublished result). In the ^{1}H-^{13}C CT-HSQC spectra recorded with these samples (Figure 3), valine CγR or leucine CδR gives a positive peak whereas their prochiral S methyl groups are of opposite sign. In this manner, 46 out of 48 methyl groups of valine and leucine in recoverin have been assigned stereospecifically. The remaining two methyls were consequently assigned stereospecifically since each chiral pair of these methyls has been assigned. For Leu^{17}, Leu^{102}, Leu^{167}, and Leu^{177}, the CδR gives a dispersive peak. This might be caused by strong coupling between Cγ and CδR resonances, though their Cγ resonances are still unassigned.

Resonance assignment of the N-terminal myristoyl group

The ^{1}H and ^{13}C signals of the myristoyl group except for those of the C4–C10 positions were well resolved in a 2D ^{1}H-^{13}C HMQC spectrum of ^{15}N-labeled recoverin with the ^{13}C-labeled myristoyl group (Figure 4). The myristoyl resonances are assigned using a 3D HCCH-COSY spectrum together with the assignment of the myristic acid dissolved in deuterated chloroform (Ames et al., 1995b). The ^{1}H and/or ^{13}C signals of C4 and C5 are distinct and assigned in the 3D [$^{13}C/F_1$]-edited [$^{13}C/F_3$]-filtered HMQC-NOESY spectrum recorded with the sample whose protein portion is labeled with ^{15}N and the myristoyl group with ^{13}C. Careful inspection of NOE data together with the calculated structures using the distance restraints derived from unambiguously assigned myristoyl signals (i.e. C2, C3, and C11–C14), made it possible to assign the remaining signals of C6–C10 (Figure 4). The stereospecific assignment of the β-methylene pro-

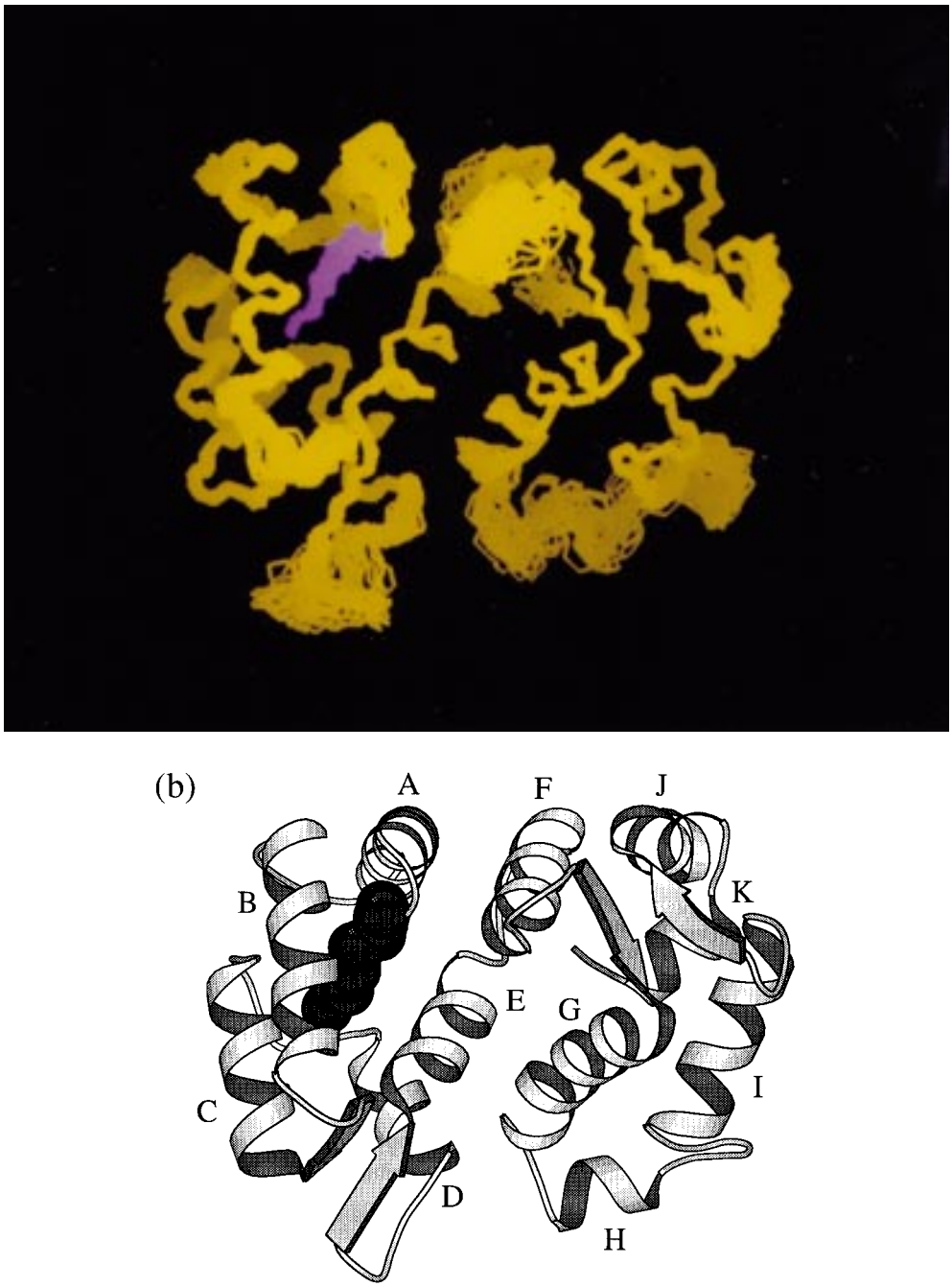

Figure 7. (a) Best-fit superposition of the backbone atoms (N, C^{α}, and C′) of the selected 30 NMR-derived structures of Ca^{2+}-free, myristoylated recoverin. The main-chain atoms of residues 1–94 of the 30 structures are superimposed against the energy-minimized average structure of residues 1–189 using the N-terminal residues which are part of regular secondary structure (residues 4–16, 25–38, 43–56, 66–73 and 80–91) with an rms deviation of 0.44 ± 0.07 Å. The main chains of residues 95–189 of the same set of structures are superimposed against the average structure using the C-terminal residues which are part of regular secondary structure (residues 98–109, 116–132, 148–159, 166–178 and 180–186) with an rms deviation of 0.33 ± 0.08 Å. The figure was generated using INSIGHT II (Biosym, San Diego, CA). (b) Ribbon diagram showing the energy-minimized average structure. Non-hydrogen atoms of the N-terminal myristoyl group are shown as a space-filling model, and the helices are labeled (see text). The model was generated using MOLSCRIPT (Kraulis, 1991).

Table 1. Structural statistics of the 30 structures of Ca^{2+}-free, myristoylated recoverin[a]

Rms deviations from experimental distance restraints (Å)	
All (3382)	0.022 ± 0.002
Interresidue sequential ($\|i - j\| = 1$) (711)	0.019 ± 0.003
Interresidue short-range ($1 < \|i - j\| \leq 5$) (570)	0.025 ± 0.004
Interresidue long-range ($\|i - j\| > 5$) (966)	0.023 ± 0.001
Intraresidue (995)	0.020 ± 0.000
H-bond (140)	0.023 ± 0.001
Rms deviations from experimental dihedral restraints (°) (297)	0.19 ± 0.037
Rms deviations from idealized covalent geometry	
Bonds (Å)	0.007 ± 0.0001
Angles (°)	2.07 ± 0.003
Impropers (°)	0.94 ± 0.001
Energies (kcal mol^{-1})	
F_{NOE}[b]	80.7 ± 8.2
F_{cdih}[b]	0.74 ± 0.54
F_{repel}[c]	22.4 ± 2.1
$E_{L\text{-}J}$[d]	–578.3 ± 22.6

[a] The number of each type of restraints used in the structure calculation is given in parentheses. None of the structures exhibit distance violations greater than 0.40 Å or dihedral angle violations greater than 3.0°.

[b] F_{NOE} and F_{cdih} were calculated using force constants of 50 kcal mol^{-1} $Å^{-2}$ and 200 kcal mol^{-1} rad^{-2}, respectively.

[c] F_{repel} was calculated using a final value of 4.0 kcal mol^{-1} $Å^{-4}$ with the van der Waals hard sphere radii set to 0.75 times those in the parameter set PARALLHSA supplied with X-PLOR (Brünger, 1992).

[d] $E_{L\text{-}J}$ is the Lennard-Jones van der Waals energy calculated with the CHARMM empirical energy function and is not included in the target function for simulated annealing calculation.

tons at C2–C5, C11, and C12 positions was also accomplished in a similar structure-assisted manner.

NOEs between the N-terminal myristoyl group and the protein

Since the ^{1}H and ^{13}C chemical shifts of the myristoyl group are severely overlapped with the protein signals, it was not straightforward to distinguish NOEs between the myristoyl group and the protein from those observed in the protein. To overcome this problem, only the myristoyl group was labeled with ^{13}C and the 3D [$^{13}C/F_1$]-edited [$^{13}C/F_3$]-filtered HMQC-NOESY spectrum was recorded (Figure 5). This experiment enabled us to extract the NOEs between the myristoyl group and the protein. Many NOE cross peaks were observed between the myristoyl protons and aromatic protons whose assignments were previously accomplished by homonuclear 2D TOCSY and NOESY experiments. It was straightforward to assign the protein–lipid NOEs by a combined use of the 3D ^{13}C-edited NOESY-HMQC and homonuclear 2D NOESY spectra. A ^{15}N-edited NOESY-HMQC spectrum also helped for the assignment. Finally, 153 NOEs between the myristoyl group and the protein were obtained.

Structure of the myristoylated protein

The 3D structure of Ca^{2+}-free, myristoylated recoverin has been determined using 3679 experimental constraints (see Table 1) derived from NMR spectroscopy. A summary of geometric and energy parameters for the refined structure is presented in Table 1. Figure 6 summarizes the distribution of NOE constraints, rms deviations for the backbone and all heavy atoms, and solvent-accessible surface areas in the 30 final structures of Ca^{2+}-free, myristoylated recoverin as a function of residue number. No violations greater than 0.40 Å and 3.0° for distance and dihedral angle restraints, respectively, were observed for any structure.

Compared to our previous study (Tanaka et al., 1995), 532 distance and 59 dihedral angle restraints

Table 2. Average rms deviations from the energy-minimized average structure of the 30 selected recoverin structures[a]

Residues used for rms deviation calculation	Average rms deviation (Å)	
	Backbone[b]	All heavy
N-terminal domain (1–94)		
α-Helices and β-sheets[c]	0.44 ±0.07	1.09 ±0.07
	(0.44±0.04)	(1.07±0.06)
Hydrophobic core[d]	0.45 ±0.08	0.80 ±0.09
	(0.48±0.10)	(0.98±0.09)
Hydrophobic core[d] and myristoyl group	0.45 ±0.08	0.79 ±0.09
	(0.49±0.09)	(0.97±0.09)
C-terminal domain (95–189)		
α-Helices and β-sheets[e]	0.33 ±0.08	0.91 ±0.06
	(0.42±0.06)	(0.99±0.07)
Hydrophobic core[f]	0.29 ±0.08	0.58 ±0.09
	(0.34±0.07)	(0.86±0.07)

[a] The corresponding values calculated for the 24 structures determined in our previous study (Tanaka et al., 1995) are indicated in parentheses for comparison.
[b] N, C^{α}, and C′.
[c] Residues 4–16, 25–38, 43–56, 66–73, and 80–91.
[d] L9, I13, L14, L19, L28, Y32, I44, F49, I52, Y53, F56, F57, A60, A66, V69, F70, F73, A75, L81, F83, Y86, V87, I88, A89, L90, H91, and M92.
[e] Residues 98–109, 116–132, 148–159, 166–178, and 180–186.
[f] L102, W104, A105, F106, L108, Y109, I117, V122, I125, V126, A128, I129, M132, A152, I155, W156, F159, L167, F172, I173, I182, L185, and I186.

were further included in this study. The definition of the secondary structure elements of the C-terminal domain was improved more notably than that of the N-terminal domain (Table 2). This is because the C-terminal domain had previously been ill-defined, while the definition of the N-terminal domain had been relatively good. A significant improvement (0.18 Å on average) was, however, seen in the hydrophobic side chains of the N-terminal domain, a majority of which form the myristoyl binding pocket. This improvement enabled us to inspect the details of the myristate–protein interactions as discussed later.

Figure 7a shows a best-fit superposition of the determined structure of recoverin. There are 11 α-helices comprising residues 4–16 (helix A), 25–38 (B), 46–56 (C), 66–73 (D), 83–91 (E), 98–109 (F), 119–132 (G), 135–140 (H), 148–159 (I), 169–178 (J), and 180–186 (K) (Figure 7b). Overall, 58% of the residues are in a helical conformation. Helices B and C form EF-1, helices D and E form EF-2, helices F and G form EF-3, and helices I and J form EF-4. The N-terminal domain consists of EF-1 and EF-2, and the C-terminal domain consists of EF-3 and EF-4. A sharply bent linker (residues 92–97) between the two domains allows the four EF-hands to form a compact linear array. This contrasts with the two independent domains seen in calmodulin (Babu et al., 1985; Kretsinger et al., 1986; Barbato et al., 1992; Kuboniwa et al., 1995; Zhang et al., 1995) and troponin C (Herzberg and James, 1988; Slupsky and Sykes, 1995). In addition to the helices, two short antiparallel β-sheets are formed between residues 43 to 45 and 80 to 82 and between residues 116 to 118 and 166 to 168. These secondary structural elements are well defined (Figure 7a and Table 2). Due to the lack of a large number of experimental distance and dihedral angle constraints, the linker between helices H and I, the EF-hand loop regions and the C-terminal 13 residues are less well defined.

Myristoyl binding pocket

The myristoyl group attached to the N-terminal glycine projects into a deep, hydrophobic pocket located in the N-terminal domain (Figure 7b). The present NMR structure defines the myristoyl binding pocket at high resolution (Figure 8). The myristoyl group is surrounded by many hydrophobic residues provided by five helices. Leu^{14} in helix A contacts

Figure 8. Hydrophobic residues surrounding the myristoyl group. (a) Selected 30 NMR-derived structures of Ca^{2+}-free, myristoylated recoverin when atoms in regular secondary structure elements are fitted as described in Figure 7a. (b) Schematic drawing of the energy-minimized average structure. Only hydrophobic residues within 5 Å of the myristoyl group (in orange) are shown and labeled with a one-letter code and a residue number. (c) Space-filling model showing side-chain atoms within 5 Å of the myristoyl group. Three different front planes were selected to show the depth of the pocket. (a) and (b) were generated using INSIGHT II and (c) was generated using MIDAS (Ferrin et al., 1988).

with the middle to tail (C14 end) portion of the myristoyl group. Helix B provides three hydrophobic residues (Leu^{28}, Trp^{31}, and Tyr^{32}) forming a cluster that interacts with the middle to head (C1 end) part of the myristoyl group. This cluster provides approximately one quarter of the total buried surface area (528 $Å^2$) of the myristoyl group. Two hydrophobic residues (Phe^{49} and Phe^{56}) of helix C and three residues (Tyr^{86}, Val^{87}, and Leu^{90}) of helix E together sandwich the myristoyl group at the tail end. These interactions are supplemented by Ile^{52} and Tyr^{53} of helix C and Phe^{83} and His^{91} of helix E. The buried surface area by those residues from helices C and E is 212 $Å^2$, equivalent to 40% of the myristoyl surface. Finally, Trp^{104} and Leu^{108} of helix F cover a part of the head portion of the myristoyl group with a buried surface area of 48 $Å^2$. All together, the myristoyl group is buried by numerous hydrophobic residues as shown in Figure 8.

Discussion and Conclusions

Three types of ^{13}C-labeled protein samples were prepared in this work (Figure 1): *a*, uniformly $^{15}N/^{13}C$-labeled recoverin with the non-labeled myristoyl group; *b*, uniformly ^{15}N-labeled recoverin with the ^{13}C-labeled myristoyl group; and *c*, uniformly ^{13}C-labeled recoverin with the ^{13}C-labeled myristoyl group. Sample *a* is mainly used for the backbone and side-chain assignments of the protein part as well as the NOE assignments within the protein. Since ^{1}H resonances of the myristoyl group were severely overlapped with the protein resonances, the introduction of ^{13}C only in the myristoyl group (sample *b*) was ex-

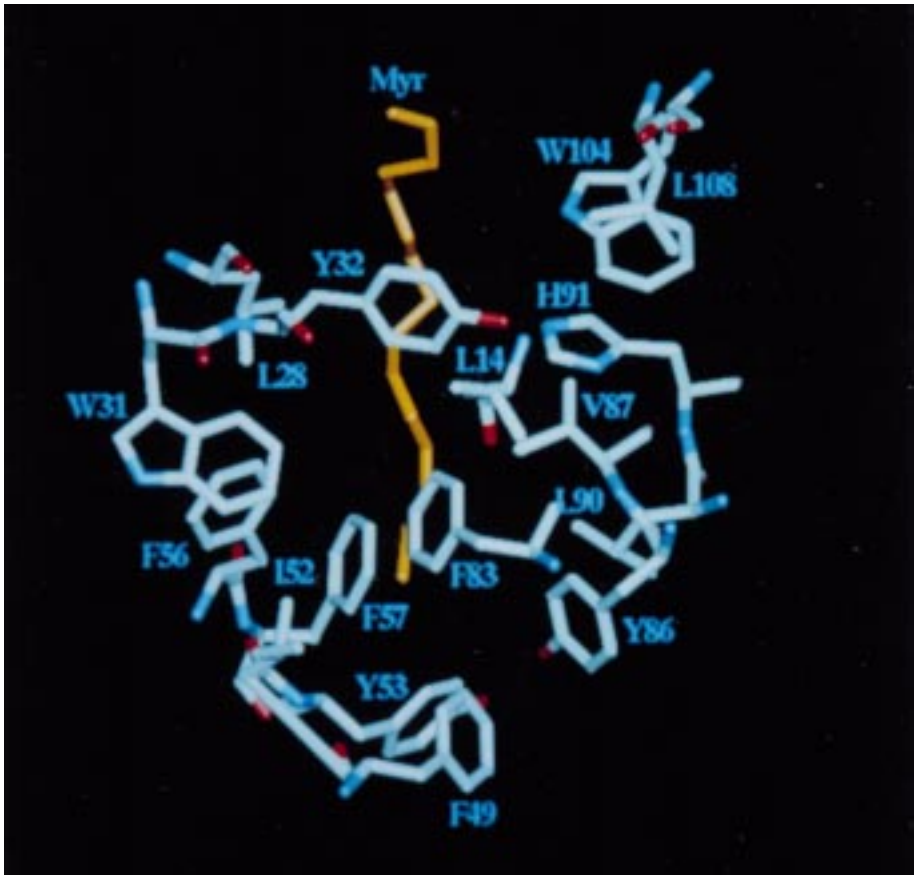

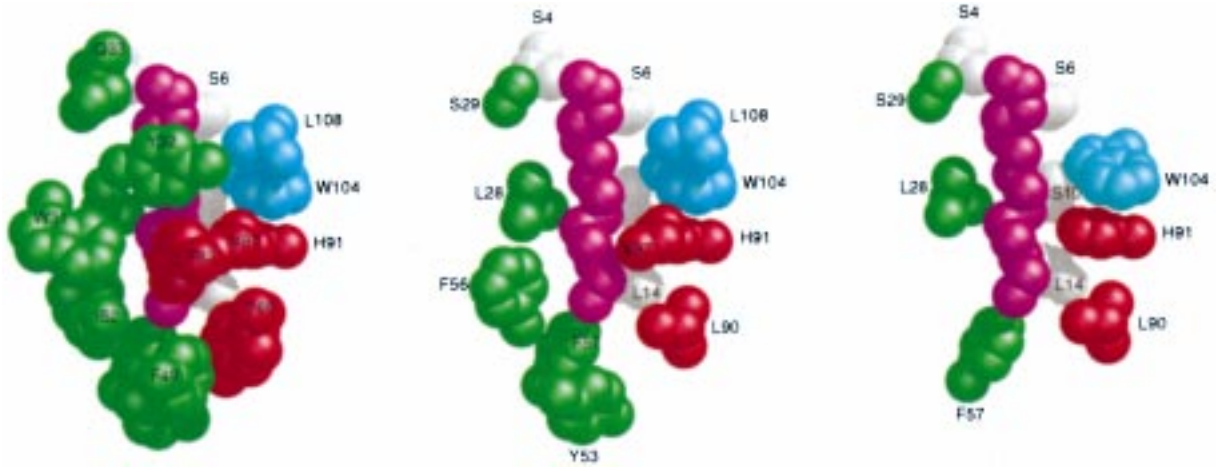

Figure 8. Continued.

Table 3. Conformation of the myristoyl group and its interaction with protein residues

Carbon atom	Torsion angle[a]	Number of observed NOEs	Protein residues with NOE contact[b]
C1			
	–158.5 ± 7.1		
C2		12	G2, N3, S6, Y32, L108
	153.6 ± 13.4		
C3		15	G2, S4, S6, S29, Y32, L36, L108
	77.1 ± 43.9		
C4		11	S4, S6, S29, Y32, L108
	169.9 ± 34.1		
C5		6	G7, S10, S29, Y32, L108
	–164.8 ± 46.9		
C6		7	G7, S10, L28, S29, Y32, W104
	–177.9 ± 73.5		
C7		3	Y32, V87
	–168.7 ± 55.9		
C8		10	S10, L14, L28, W31, Y32, V87, W104
	175.0 ± 62.5		
C9		6	L28, W31, Y32, V87
	–151.1 ± 47.2		
C10		8	L14, L28, W31, Y32, V87
	–167.4 ± 25.8		
C11		12	L14, L28, F57, F83, V87, H91
	142.5 ± 32.6		
C12		21	L14, W31, Y32, I52, F56, F57, F83, Y86, V87, H91
	–176.0 ± 17.9		
C13		16	L14, I52, Y53, F56, F57, F83, Y86, V87, L90
C14		26	L14, W31, F49, I52, Y53, F56, F57, A66, F83, Y86, L108, V111

[a] Calculated using the 30 NMR-derived structures.
[b] The residues whose backbone protons show NOEs with the myristoyl group are underlined.

tremely useful to assign the myristate resonances and to extract the myristate–protein NOEs. These NOEs assigned in the 3D $[^{13}C/F_1]$-edited $[^{13}C/F_3]$-filtered HMQC-NOESY spectrum made it possible to define the structure of the myristoyl binding site. Sample *c* was used to confirm the NOE assignments obtained using the other two samples. It is noted that without this sample the NOE assignments associated with leucine residues were impossible due to an unexpected scrambling during the protein expression (see below). A combined use of the three protein samples was essential for the structure determination of the myristoylated recoverin.

The present study represents the first example of high-resolution NMR structure determination of a myristoylated protein. The refined structure provides a better picture of the hydrophobic pocket essential for sequestering the N-terminal myristoyl group. The myristoyl binding pocket in the present structure comprises well-defined side-chain groups as illustrated in Figure 8. In contrast, the 14 carbon containing myristoyl chain itself is less defined. The terminal nuclei C1 and C14 are better defined than the central portion (C6–C8) (Table 3), consistent with the number of NOEs observed at each site. The use of pseudo-atom corrections (1.5 or 2.0 Å) employed for methyl and aromatic groups in the protein is also responsible for the resolution of the structure. Nevertheless, it is interesting to note that the myristoyl group is not fully extended: the average distance between C1 and C14 atoms of the myristoyl group in the present structure is 14.6 (±0.3) Å, whereas the corresponding distance in its all-trans form is 16.2 Å and 12.9 Å for the J-shaped myristoyl group of cAMP-dependent protein kinase (Zheng et al., 1993). This indicates that the hydrophobic pocket is rather small in depth for a fully extended

myristoyl chain and could fit other acyl groups such as C12:0, C14:1, and C14:2 chains found in native recoverin isolated from bovine retina (Johnson et al., 1994).

A concave hydrophobic surface found in the crystal structure of one-Ca^{2+}-bound, unmyristoylated recoverin was thought to be a putative binding site of the N-terminal myristoyl group (Flaherty et al., 1993). The aromatic and aliphatic residues forming the hydrophobic crevice are mainly contributed from three helices: Trp^{31} from helix B; Ile^{52}, Tyr^{53}, and Phe^{56} from helix C; Tyr^{86} and Leu^{90} from helix E. A majority of the hydrophobic residues found in the concave surface of the Ca^{2+}-bound structure indeed participate in the hydrophobic pocket in the N-terminal domain of Ca^{2+}-free recoverin. However, many other hydrophobic residues (Leu^{14} in helix A, Leu^{28} and Tyr^{32} in helix B, Phe^{49} in helix C, Phe^{83}, Val^{87}, and His^{91} in helix E, Trp^{104} and Leu^{108} in helix F) also come close in the Ca^{2+}-free state to constitute the deep myristoyl binding pocket.

Our first attempt to make uniformly ^{13}C-labeled recoverin unexpectedly yielded an extremely low ^{13}C enrichment for leucine. In this preparation non-labeled myristic acid was added to the cell culture containing $^{13}C_6$-glucose about 2 h prior to the induction of NMT that catalyzes myristoylation at the N-terminal glycine. The low ^{13}C enrichment for leucine was completely abolished when uniformly ^{13}C-labeled myristic acid was added to the ^{13}C-enriched cell culture. A possible intermediate responsible for this scrambling is pyruvic acid, which can be produced in the glyoxylate cycle from acetyl-CoA, a key metabolic intermediate in fatty acid synthesis. It is, however, hard to understand that such a scrambling occurred only for leucine, since pyruvic acid is used in the synthesis of most, if not all, amino acids. These results suggest an unknown pathway generating a leucine precursor from myristic acid in *E. coli.*

The interhelical angles of the two helices of EF-1 (167°), EF-3 (119°), and EF-4 (96°) in the Ca^{2+}-free recoverin (Table 4) are very different from other values (130–140°) for the known closed conformation of Ca^{2+}-free EF-hands in calmodulin (Zhang et al., 1995) and troponin C (Herzberg and James, 1988). The abnormally large value of EF-1 might be a consequence of this EF-hand being a major contributor to the binding site of the myristoyl group. The presence of Pro^{40} and the absence of two essential acidic residues at the X and Y positions in the Ca^{2+}-binding loop might be also responsible for the nearly antiparallel helix packing of EF-1. The interhelical angles of EF-3 and EF-4 are rather close to the values for the open conformation (90–110°) found in Ca^{2+}-bound EF-hands of calmodulin (Babu et al., 1988) and troponin C (Herzberg and James, 1988). The midpoint distances between the two helices of EF-3 and EF-4 are both approximately 15 Å (Table 4), the similar value found in Ca^{2+}-bound calmodulin (15 Å for EF-3 and 14 Å for EF-4). Two extra helices (helix H and helix K) in the C-terminal domain might be responsible for the 'semi-open' conformation of EF-3 and EF-4.

Table 4. Interhelix angles and axial separations between pairs of helices in Ca^{2+}-free myristoylated recoverin[a]

Helix pair		Interhelix angle (axial separation)
N-terminal domain	A/B	103 ± 2 (13.3 ± 0.2)
	A/E	53 ± 2 (13.1 ± 0.2)
	B/C	167 ± 2 (14.9 ± 0.3)
	D/E	132 ± 3 (10.6 ± 0.2)
	C/D	155 ± 3 (12.6 ± 0.2)
	B/E	145 ± 2 (14.7 ± 0.2)
C-terminal domain	F/G	119 ± 2 (14.5 ± 0.2)
	I/J	96 ± 1 (14.7 ± 0.1)
	G/I	130 ± 3 (10.5 ± 0.3)
	F/J	148 ± 3 (10.3 ± 0.1)
Domain interface	A/F	139 ± 3 (10.0 ± 0.3)
	D/F	47 ± 4 (21.8 ± 0.3)
	D/G	108 ± 3 (16.6 ± 0.3)
	E/F	168 ± 3 (12.7 ± 0.2)
	E/G	74 ± 2 (10.4 ± 0.2)

[a] The interhelix angle (°) between each helical pair is followed by the axial separation (Å) in parentheses. Calculated using the 30 NMR-derived structures by an in-house program written by K. Yap.

A number of recently discovered recoverin homologues are likely to regulate membrane-bound proteins through a Ca^{2+}-myristoyl switch. Other myristoylated or acylated proteins include ADP-ribosylation factors (ARF) (Franco et al., 1996), myristoylated alanine-rich C kinase substrate (MARCKS) (McLaughlin and Aderem, 1995), nitric oxide synthase (Michel et al., 1993), members of Src tyrosine kinase (Resh, 1994), and guanine nucleotide binding protein (G protein) (Jones et al., 1990). These proteins all interact with membranes and play a role in cellular signaling processes, but little is known about atomic resolution structural information of their acyl groups in these proteins. Other membrane-associated signaling proteins including members of the ras superfamily (rabs,

rho, and rac) and photoreceptor proteins (transducin, rhodopsin kinase, and RGS protein) are modified by prenyl and/or palmitoyl lipid groups (Inglese et al., 1992; Milligan et al., 1995; Wedegaertner et al., 1995). No structural information is known for the lipidated forms of these proteins. The NMR strategy described here is applicable to lipidated proteins in general.

Acknowledgements

We thank C. Tan for synthesizing the ^{13}C-labeled myristic acid, L. Kay for providing NMR pulse sequence programs, F. Delaglio and D. Garrett for providing computer software for NMR data processing and analysis, T. Harvey for providing the topology and parameter files of the myristoyl group, and T. Neubert for doing mass spectrometry analysis on the myristoylated recoverin samples. This work was supported by a grant to M.I. from the Medical Research Council of Canada, and grants to L.S. from the National Institutes of Health (NIH) (GM24032 and EY02005). T.T. and J.B.A. were supported by Ontario Cancer Institute/Amgen and NIH postdoctoral fellowships, respectively. M.I. is a Howard Hughes International Research Scholar and a Medical Research Council of Canada Scholar.

References

Ames, J.B., Tanaka, T., Stryer, L. and Ikura, M. (1994) *Biochemistry*, **33**, 10743–10753.

Ames, J.B., Porumb, T., Tanaka, T., Ikura, M. and Stryer, L. (1995a) *J. Biol. Chem.*, **270**, 4526–4533.

Ames, J.B., Tanaka, T., Ikura, M. and Stryer, L. (1995b) *J. Biol. Chem.*, **270**, 30909–30913.

Archer, S.J., Ikura, M., Torchia, D.A. and Bax, A. (1991) *J. Magn. Reson.*, **95**, 636–641.

Babu, Y.S., Sack, J.S., Greenhough, T.J., Bugg, C.E., Means, A.R. and Cook, W.J. (1985) *Nature*, **315**, 37–40.

Babu, Y.S., Bugg, C.E. and Cook, W.J. (1988) *J. Mol. Biol.*, **204**, 191–204.

Bagby, S., Harvey, T.S., Eagle, S.G., Inouye, S. and Ikura, M. (1994) *Structure*, **2**, 107–122.

Barbato, G., Ikura, M., Kay, L.E., Pastor, R.W. and Bax, A. (1992) *Biochemistry*, **31**, 5269–5278.

Bax, A., Clore, G.M. and Gronenborn, A.M. (1990) *J. Magn. Reson.*, **88**, 425–431.

Bax, A. and Pochapsky, S.S. (1992) *J. Magn. Reson.*, **99**, 638–643.

Bendall, M.R., Pegg, D.T. and Doddrell, D.M. (1983) *J. Magn. Reson.*, **52**, 81–117.

Braunschweiler, L. and Ernst, R.R. (1983) *J. Magn. Reson.*, **53**, 521–528.

Brünger, A.T. (1992) *X-PLOR Version 3.1: A System for X-ray Crystallography and NMR*, Yale University Press, New Haven, CT.

Chen, C.K., Inglese, J., Lefkowitz, R.J. and Hurley, J.B. (1995) *J. Biol. Chem.*, **270**, 18060–18066.

Clore, G.M., Gronenborn, A.M., Nilges, M. and Ryan, C.A. (1987) *Biochemistry*, **26**, 8012–8023.

Clore, G.M., Bax, A. and Gronenborn, A.M. (1991) *J. Biomol. NMR*, **1**, 13–22.

Delaglio, F. (1993) NMRPipe system of software, National Institutes of Health, Bethesda, MD.

Dizhoor, A.M., Ericsson, L.H., Johnson, R.S., Kumar, S., Olshevskaya, E., Zozulya, S., Neubert, T.A., Stryer, L., Hurley, J.B. and Walsh, K.A. (1992) *J. Biol. Chem.*, **267**, 16033–16036.

Dizhoor, A.M., Chen, C.-K., Olshevskaya, E., Sinelnikova, V.V., Phillipov, P. and Hurley, J.B. (1993) *Science*, **259**, 829–832.

Driscoll, P.C., Gronenborn, A.M. and Clore, G.M. (1989) *FEBS Lett.*, **243**, 223–233.

Ferrin, T.E., Huang, C.C., Jarvis, L.E. and Langridge, R. (1988) *J. Mol. Graph.*, **6**, 13–27.

Flaherty, K.M., Zozulya, S., Stryer, L. and McKay, D.B. (1993) *Cell*, **75**, 709–716.

Franco, M., Chardin, P., Chabre, M. and Paris, S. (1996) *J. Biol. Chem.*, **271**, 1573–1578.

Garrett, D.S., Powers, R., Gronenborn, A.M. and Clore, G.M. (1991) *J. Magn. Reson.*, **95**, 214–220.

Gray-Keller, M.P., Polans, A.S., Palczewski, K. and Detwiler, P.B. (1993) *Neuron*, **10**, 523–531.

Herzberg, O. and James, M.N.G. (1988) *J. Mol. Biol.*, **203**, 761–779.

Hughes, R.E., Brzovic, P.S., Klevit, R.E. and Hurley, J.B. (1995) *Biochemistry*, **34**, 11410–11416.

Ikura, M., Kay, L.E. and Bax, A. (1991) *J. Biomol. NMR*, **1**, 299–304.

Inglese, J., Koch, W.J., Caron, M.G. and Lefkowitz, R.J. (1992) *Nature*, **359**, 147–150.

Jeener, J., Meier, B.H., Bachmann, P. and Ernst, R.R. (1979) *J. Chem. Phys.*, **71**, 4546–4553.

Johnson, R.S., Ohguro, H., Palczewski, K., Hurley, J.B., Walsh, K.A. and Neubert, T.A. (1994) *J. Biol. Chem.*, **269**, 21067–21071.

Jones, T.L.Z., Simonds, W.F., Merendino Jr., J.J., Brann, M.R. and Spiegel, A.M. (1990) *Proc. Natl. Acad. Sci. USA*, **87**, 568–572.

Kawamura, S. (1993) *Nature*, **362**, 855–857.

Kawamura, S., Hisatomi, O., Kayada, S., Tokunaga, F. and Kuo, C.-H. (1993) *J. Biol. Chem.*, **268**, 14579–14582.

Kay, L.E. and Bax, A. (1990) *J. Magn. Reson.*, **86**, 110–126.

Kay, L.E., Keifer, P. and Saarinen, T. (1992) *J. Am. Chem. Soc.*, **114**, 10663–10665.

Kay, L.E., Xu, G.Y., Singer, A.U., Muhandiram, D.R. and Forman-Kay, J.D. (1993) *J. Magn. Reson.*, **B101**, 333–337.

Klenchin, V.A., Calvert, P.D. and Bownds, M.D. (1995) *J. Biol. Chem.*, **270**, 16147–16152.

Kobayashi, M., Takamatsu, K., Saitoh, S., Miura, M. and Noguchi, T. (1992) *Biochem. Biophys. Res. Commun.*, **189**, 511–517.

Kobayashi, M., Takamatsu, K., Saitoh, S. and Noguchi, T. (1993) *J. Biol. Chem.*, **268**, 18898–18904.

Kraulis, P.J. (1991) *J. Appl. Crystallogr.*, **24**, 946–950.

Kretsinger, R.H., Rudnick, S.E. and Weissman, L.J. (1986) *J. Inorg. Biochem.*, **28**, 289–302.

Kuboniwa, H., Tjandra, N., Grzesiek, S., Ren, H., Klee, C.B. and Bax, A. (1995) *Nat. Struct. Biol.*, **2**, 768–776.

Kuno, T., Kajimoto, Y., Hashimoto, T., Mukai, H., Shirai, Y., Saheki, S. and Tanaka, C. (1992) *Biochem. Biophys. Res. Commun.*, **184**, 1219–1225.

Ladant, D. (1995) *J. Biol. Chem.*, **270**, 3179–3185.

Lee, W., Revington, M.J., Arrowsmith, C. and Kay, L.E. (1994) *FEBS Lett.*, **350**, 87–90.

McLaughlin, S. and Aderem, A. (1995) *Trends Biochem. Sci.*, **20**, 272–276.
Michel, T., Li, G.K. and Busconi, L. (1993) *Proc. Natl. Acad. Sci. USA*, **90**, 6252–6256.
Milligan, G., Parenti, M. and Magee, A.I. (1995) *Trends Biochem. Sci.*, **20**, 181–186.
Muhandiram, D.R., Farrow, N.A., Xu, G.-Y., Smallcombe, S.H. and Kay, L.E. (1993) *J. Magn. Reson.*, **B102**, 317–321.
Nilges, M., Gronenborn, A.M., Brünger, A.T. and Clore, G.M. (1988) *Protein Eng.*, **2**, 27–38.
Pascal, S.M., Muhandiram, D.R., Yamazaki, T., Forman-Kay, J.D. and Kay, L.E. (1994) *J. Magn. Reson.*, **B103**, 197–201.
Pongs, O., Lindemeier, J., Zhu, X.R., Theil, T., Engelkamp, D., Krah-Jentgens, I., Lambrecht, H.-G., Koch, K.W., Schwemer, J., Rivosecchi, R., Mallart, A., Galceran, J., Canal, I., Barbas, J.A. and Ferrus, A. (1993) *Neuron*, **11**, 15–28.
Resh, M.D. (1994) *Cell*, **76**, 411–413.
Shaka, A.J., Keeler, J., Frenkiel, T.A. and Freeman, R. (1983) *J. Magn. Reson.*, **52**, 335–338.
Slupsky, C.M. and Sykes, B.D. (1995) *Biochemistry*, **34**, 15953–15964.
Tanaka, T., Ames, J.B., Harvey, T.S., Stryer, L. and Ikura, M. (1995) *Nature*, **376**, 444–447.
Tate, S., Ushioda, T., Utsunomiya-Tate, N., Shibuya, K., Ohyama, Y., Nakano, Y., Kaji, H., Inagaki, F., Samejima, T. and Kainosho, M. (1995) *Biochemistry*, **34**, 14637–14648.
Terasawa, M., Nakano, A., Kobayashi, R. and Hidaka, H. (1992) *J. Biol. Chem.*, **267**, 19596–19599.
Towler, D.A., Adams, S.P., Eubanks, S.R., Towery, D.S., Jakson-Machelski, E., Glaser, L. and Gordon, J.I. (1988) *J. Biol. Chem.*, **263**, 1784–1790.
Vuister, G.W. and Bax, A. (1992) *J. Magn. Reson.*, **98**, 428–435.
Wagner, G., Braun, W., Havel, T.F., Schaumann, T., Gō, N. and Wüthrich, K. (1987) *J. Mol. Biol.*, **196**, 611–639.
Wedegaertner, P.B., Wilson, P.T. and Bourne, H.R. (1995) *J. Biol. Chem.*, **270**, 503–506.
Wishart, D.S. and Sykes, B.D. (1994) *Methods Enzymol.*, **239**, 363–392.
Wüthrich, K., Billeter, M. and Braun, W. (1983) *J. Mol. Biol.*, **169**, 949–961.
Wüthrich, K. (1986) *NMR of Proteins and Nucleic Acids*, Wiley, New York, NY.
Yamagata, K., Goto, K., Kuo, C.-H., Kondo, H. and Miki, N. (1990) *Neuron*, **2**, 469–476.
Yamazaki, T., Forman-Kay, J.D. and Kay, L.E. (1993) *J. Am. Chem. Soc.*, **115**, 11054–11055.
Zhang, M., Tanaka, T. and Ikura, M. (1995) *Nat. Struct. Biol.*, **2**, 758–767.
Zhang, O., Kay, L.E., Olivier, J.P. and Forman-Kay, J.D. (1994) *J. Biomol. NMR*, **4**, 845–858.
Zheng, J., Knighton, D.R., Xuong, N.-H., Taylor, S.S., Sowadski, J.M. and Ten Eyck, L.F. (1993) *Protein Sci.*, **2**, 1559–1573.
Zozulya, S. and Stryer, L. (1992) *Proc. Natl. Acad. Sci. USA*, **89**, 11569–11573.